Tidal Love numbers of axion stars

Jun-Ru Chen, Long-Xing Huang, Li Zhao, and Yong-Qiang Wang*

Lanzhou Center for Theoretical Physics, Key Laboratory of Theoretical Physics of Gansu Province, School of Physical Science and Technology, Lanzhou University, Lanzhou 730000, China and Institute of Theoretical Physics & Research Center of Gravitation, Lanzhou University, Lanzhou 730000, China

(Received 29 November 2023; accepted 10 April 2024; published 30 May 2024)

We investigate spherically symmetric axion stars with minimal coupling between a complex scalar field and gravity in a tidal environment. Tidal perturbations are treated as linear, and we calculate the tidal Love numbers for axion stars. The results show that the electric Love numbers of axion stars are positive, while the magnetic Love numbers are negative on the stable branch. The electric tidal Love numbers are much larger than the magnetic ones on the Newtonian stable branch, but only slightly larger on the relativistic stable branch. The relativistic stable branch has much smaller tidal Love numbers than the Newtonian stable branch, indicating weaker deformability of axion stars on the relativistic stable branch. This is due to the fact that axion stars are more compact on the relativistic branch, and thus hardly distorted by tidal forces.

DOI: 10.1103/PhysRevD.109.104078

I. INTRODUCTION

In an external tidal environment, the uneven gravitational fields and the relative motion between the bodies cause tidal effects, which are fundamental in astrophysics as they reveal the interactions and deformability of gravitational objects. Tidal effects can alter the rotational speeds of gravitational objects, giving rise to astrophysical phenomena such as tidal tails and tidal locking [1,2].

Ocean tide in the Earth-Moon system is the most well-known tidal phenomenon. It causes periodic rise and fall of the ocean surface, creates tidal friction, and affects the Earth's rotation rate, resulting in a slower rotation rate. To characterize Earth's response to tidal forces, Love introduced the concept of Love numbers in Newtonian gravity, introducing two dimensionless parameters, denoted as h and k [3]. The h describes the relative longitudinal deformation, while k delineates the relative deformation in the gravitational potential [4]. Later, the third dimensionless parameter, l, was introduced by Shida to account for the relative horizontal deformation of the Earth, which is called Shida number sometimes [5]. Collectively, these three dimensionless parameters are recognized as the Love numbers.

The prospects of observing the tidal Love numbers of spherically symmetric neutron stars have motivated the study of the tidal Love numbers in general relativity [6–9]. Tidal deformation can affect the waveform of gravitational waves, which is related to the internal structure of neutron stars [7]. By measuring the tidal Love numbers through gravitational wave observations, we can constrain the equation of state that governs the interiors of neutron stars [10,11]. In the relativistic theory, the key deformation parameter is k, which is related to the ratio between the multipole moments induced by deformations and the multipole moment of the tidal field [8,9]. In terms of parity, Love numbers are classified into even Love numbers (electric type) and odd Love numbers (magnetic type). The discovery of the I-Love-Q relations for slowly rotating neutron stars has provided a novel avenue for inferring the other two physical quantities through tidal Love numbers, and can test general relativity in the strong-field regime [12,13]. Furthermore, research efforts have extended to investigate tidal deformations in rotating compact objects [14–20]. Additionally, calculations of tidal Love numbers have been explored within modified gravity [21,22].

Afterward, the study about tidal deformation of black holes has yielded an intriguing result that for Schwarzschild black holes both their electric and magnetic Love numbers are found to be zero [8,9,23]. Subsequently, similar conclusions have been extended to slowly rotating black holes [14,17,24,25]. In other words, under the influence of tidal forces, there is no generation of induced multipole moments, thereby leaving the multipolar structure of the black hole unaltered. Although the gravitational field of a black hole is extremely strong, due to its singularity and lack of actual material structure, it cannot generate tidal deformation, which is significantly different from other self-gravitational objects. The tidal Love numbers within the gravitational wave signal during the binary inspiral can be used to test the properties of black holes and distinguish them from other compact objects to some extent [26–28].

*Corresponding author: yqwang@lzu.edu.cn

 © 2024 American Physical Society

Boson stars (BSs) as compact stars different from black holes are solitonic formed by self-gravitating bosonic fields. The theoretical framework for these configurations, involving Einstein gravity coupled to a complex scalar field, was constructed by Wheeler then Kaup and Ruffini *et al.* found stable solutions for such systems [29–31]. In astrophysics, BSs are considered as candidates for dark matter [32–35]. The research indicates that the tidal Love numbers of BSs are smaller than those of neutron stars [26,36]. Moreover, there have been studies computing tidal Love numbers for Proca stars, which are vector bosonic stars, along with a rudimentary comparison with the results for scalar BSs. Spherical bosonic binary stars with the same compactness exhibit differences in the gravitational wave signals between scalar and vector during the inspiral [37]. Furthermore, investigations into the tidal Love numbers have extended to other exotic compact objects, including gravastars [38,39] and quark stars [40,41].

Axion stars are compact objects formed by axion fields, which consider a self-interaction complex scalar field minimally coupled to gravity, and are also considered one of the candidates for dark matter [42–45]. In response to the strong CP problem in quantum chromodynamics (QCD), the Peccei-Quinn mechanism was proposed, introducing the axion as a novel particle [46–49], considered as weakly interacting ultralight bosons beyond Standard Model [50]. Axionlike particles as particles beyond the Standard Model play a pivotal role in string theory models [51,52]. Spherically symmetric axion star solutions and stability analysis were studied in [53] which found new stability branches emerging at high density. Recent studies have explored rotating axion stars [54] and the multifield involving rotating axion stars mixed with boson fields [55]. Our work primarily focuses on the tidal deformability of spherically symmetric axion stars. Through numerical calculations, we have investigated the quadrupole and octupole tidal Love numbers of axion stars under various parameters f_a.

The paper is organized as follows. In Sec. II, we briefly review the model of axion stars, considering complex scalar field minimally coupled to Einstein's gravity. In Sec. III, we present the perturbation equations for axion stars, divided into odd and even perturbations. In Sec. IV, we show the numerical results of quadrupole and octupole tidal Love numbers for axion stars under different decay constants. Finally, Sec. V is our conclusion and discussion. We adopt the signature $(-,+,+,+)$ for the metric and natural units $\hbar = c = G = 1$.

II. SPHERICALLY SYMMETRIC AXION STARS

A. Model

Under the Einstein-Klein-Gordon theory, we consider the complex scalar field minimally couples with gravity, and the action is [56]

$$\mathcal{S} = \int d^4x\sqrt{-g}\left[\frac{R}{16\pi} - g^{\alpha\beta}\partial_\alpha\Psi^*\partial_\beta\Psi - V(|\Psi|^2)\right], \quad (1)$$

where R represents the Ricci scalar, Ψ denotes the axion field, Ψ^* is the complex conjugate of Ψ, g is the determinant of the metric tensor $g_{\alpha\beta}$, and $V(|\Psi|^2)$ is the scalar potential. From Eq. (1), we derive the corresponding equations of motion. Taking the variation with respect to the metric $g_{\alpha\beta}$ yields the Einstein field equation,

$$R_{\alpha\beta} - \frac{1}{2}g_{\alpha\beta}R = 8\pi T_{\alpha\beta}. \quad (2)$$

Here, the energy-momentum tensor $T_{\alpha\beta}$ for the axion field is given by

$$T_{\alpha\beta} = \partial_\alpha\Psi^*\partial_\beta\Psi + \partial_\beta\Psi^*\partial_\alpha\Psi - g_{\alpha\beta}(g^{\mu\nu}\partial_\mu\Psi^*\partial_\nu\Psi + V). \quad (3)$$

Variation with respect to the axion field Ψ yields the Klein-Gordon equation

$$\Box\Psi = \frac{\partial V}{\partial|\Psi|^2}\Psi. \quad (4)$$

According to Noether's theorem, the action of a field remains invariant under U(1) transformations, where $\Psi \to \Psi e^{i\alpha}$, with α being a constant. This implies the existence of a conserved current

$$j^\alpha = -i(\Psi^*\partial^\alpha\Psi - \Psi\partial^\alpha\Psi^*), \quad (5)$$

which satisfies $\nabla_\alpha j^\alpha = 0$. The integral of the timelike component of the four-current on a spacelike hypersurface Ω yields a conserved quantity, the Noether charge

$$Q = \int_\Omega j^t. \quad (6)$$

We consider a spherically symmetric static background, within the following metric ansatz

$$ds^2 = -e^{\eta(r)}dt^2 + e^{\xi(r)}dr^2 + r^2(d\theta^2 + \sin^2\theta d\varphi^2). \quad (7)$$

The metric is static, and the functions $\eta(r)$ and $\xi(r)$ depend only on the radial coordinate r. Using the ansatz of scalar field

$$\Psi^{(0)} = \psi_0(r)e^{-i\omega t}, \quad (8)$$

where ψ_0 is a real scalar and ω represents the angular frequency of the scalar field. The axion potential is [53,57]

$$V(\psi_0) = \frac{2\mu^2 f_a^2}{B}\left[1 - \sqrt{1 - 4B\sin^2\left(\frac{\psi_0}{2f_a}\right)}\right]. \quad (9)$$

Here, B is a constant related to the ratio of the up quark mass m_u to the down quark mass m_d, with $m_u/m_d \approx 0.48$, giving $B \approx 0.22$, μ and f_a are two free parameters. In this potential, the second term corresponds to the QCD axion effective potentials [57], and the addition of a constant term ensures $V(0) = 0$, to construct asymptotically flat axion stars. Expanding the potential around $\psi_0 = 0$,

$$V(\psi_0) = \mu^2\psi_0^2 - \left(\frac{3B-1}{12}\right)\frac{\mu^2}{f_a^2}\psi_0^4 + \cdots. \tag{10}$$

It can be observed that μ represents the mass of the axion, while f_a denotes the decay constant of the axion field. When $f_a \gg \psi_0$, only the free scalar potential remains, and the axion stars model reduces to the miniboson stars [30,31]. Taking the axion potential into Eqs. (2) and (4), we obtain a set of ordinary differential equations,

$$\eta'(r) = \frac{-1+e^{\xi(r)}}{r} + 8e^{-\eta(r)+\xi(r)}\pi r\omega^2\psi_0(r)^2 + 8\pi r\psi_0'(r)^2 + \frac{16e^{\xi(r)}f_a^2\pi r\mu^2\left(-1+\sqrt{1-2B+2B\cos\left(\frac{\psi_0(r)}{f_a}\right)}\right)}{B}, \tag{11}$$

$$\xi'(r) = \frac{1-e^{\xi(r)}}{r} + 8e^{-\eta(r)+\xi(r)}\pi r\omega^2\psi_0(r)^2 + 8\pi r\psi_0'(r)^2 - \frac{16e^{\xi(r)}f_a^2\pi r\mu^2\left(-1+\sqrt{1-2B+2B\cos\left(\frac{\psi_0(r)}{f_a}\right)}\right)}{B}, \tag{12}$$

$$\psi_0''(r) = -e^{-\eta(r)+\xi(r}\omega^2\psi_0(r) - \frac{2\psi_0'(r)}{r} - \frac{1}{2}\eta'(r)\psi_0'(r) + \frac{1}{2}\xi'(r)\psi_0'(r) + \frac{e^{\xi(r)}f_a\mu^2\sin\left(\frac{\psi_0(r)}{f_a}\right)}{\sqrt{1-2B+2B\cos\left(\frac{\psi_0(r)}{f_a}\right)}}. \tag{13}$$

B. Numerical solution

By providing appropriate boundary conditions, we can numerically solve Eqs. (11)–(13). At the origin,

$$\xi(0) = 0, \qquad \eta(0)' = 0, \qquad \psi_0'(0) = 0. \tag{14}$$

Boundary conditions at infinity

$$\lim_{r\to\infty}\eta(r) = 0, \qquad \lim_{r\to\infty}\psi_0(r) = 0. \tag{15}$$

In spherically symmetric static spacetime, when $r \to \infty$ the ADM mass of the axion stars $M = m(r \to \infty)$ can be determined using the formula

$$m(r) = \frac{r}{2}\left(1 - \frac{1}{e^{\xi(r)}}\right). \tag{16}$$

As axion stars do not have a rigid surface like neutron stars because the field function is distributed throughout space and decays exponentially, we define the effective

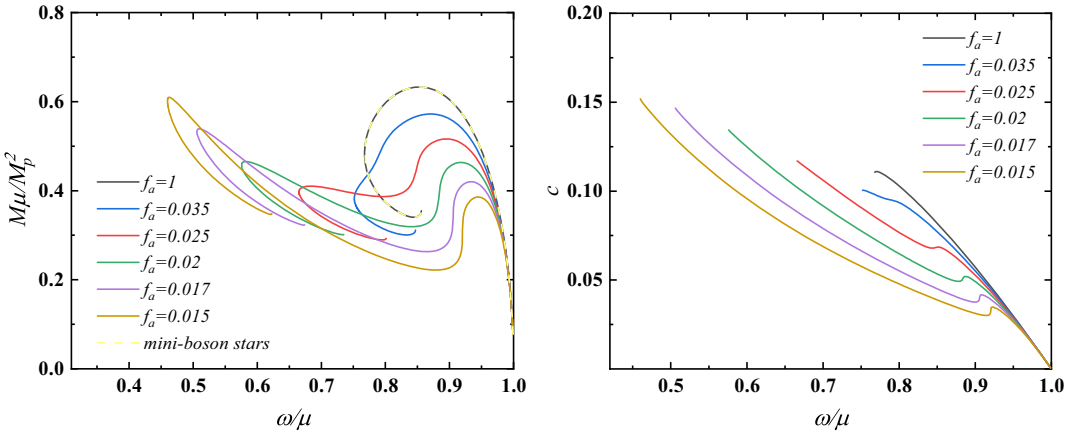

FIG. 1. Domain of existence of the axion star solutions for different decay constant f_a in an ADM mass/compactness vs frequency. Left panel: ADM mass M vs scalar field frequency ω diagram, where M is in units of M_p^2/μ and ω in units of μ. The solution for miniboson stars is represented by the yellow dotted line. Right panel: compactness c of axion stars as a function of scalar field frequency ω. Using solid lines of the same color represents the same value of f_a.

radius R of an axion star as the radius that contains 99% of the total mass [58], i.e., $m(R) = 0.99M$, and we define the compactness parameter of the axion stars as $c = M/R$.

In numerical calculations, we perform a radial coordinate transformation,

$$x = \frac{r}{1+r}, \tag{17}$$

where the radial coordinate $r \in [0, \infty)$ and the new radial coordinate $x \in [0, 1)$. Numerical solutions are obtained through the finite element method. The number of grid

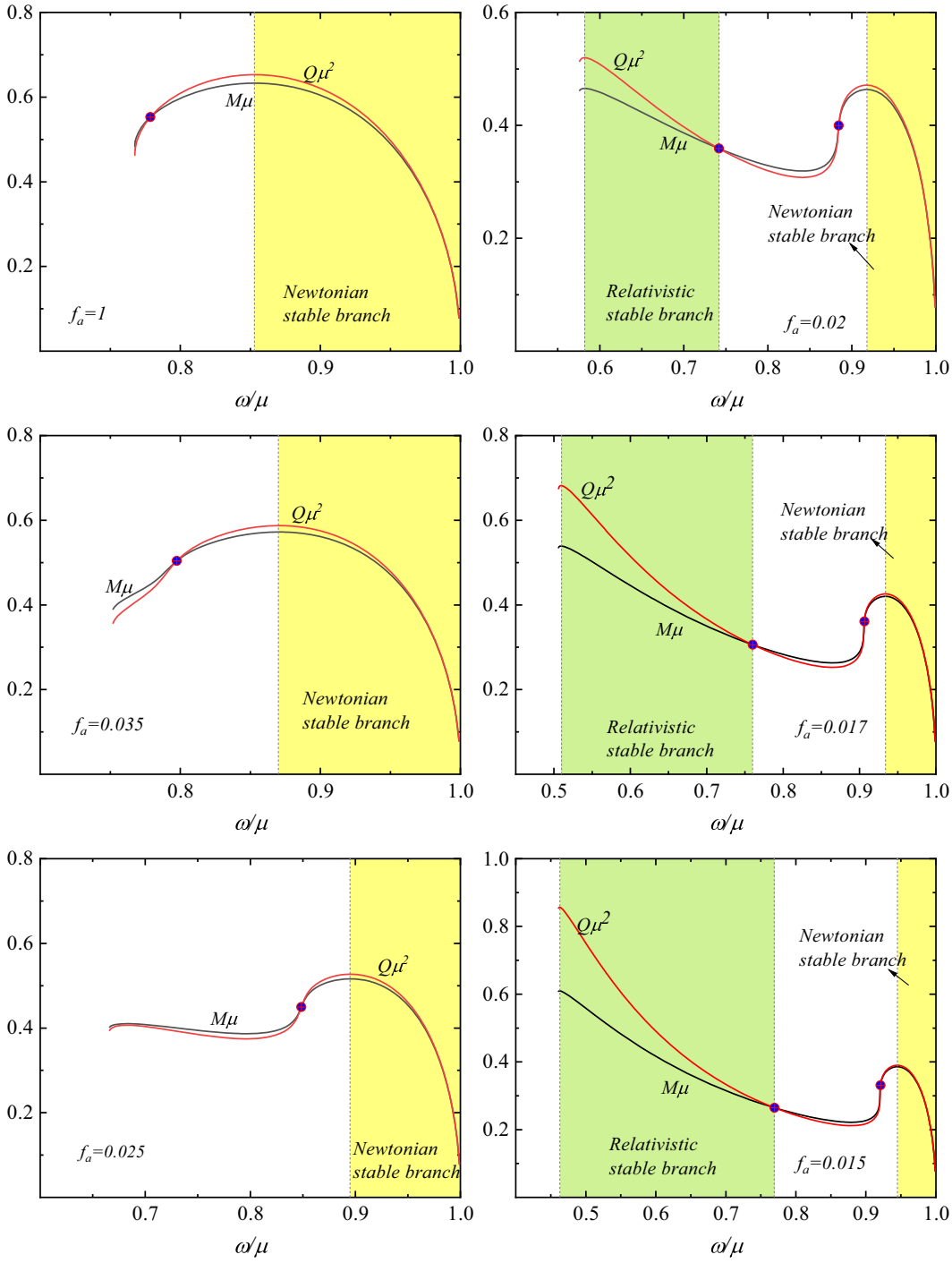

FIG. 2. Domain of existence of the axion stars for both the ADM mass and Noether charge with $f_a = \{1, 0.035, 0.025, 0.02, 0.017, 0.015\}$. The red solid line represents the Noether charge, while the black solid line represents the ADM mass.

points is 1000 in the integration region $0 \leq x < 1$. To ensure the accuracy of the computational results, we require that the relative error is less than 10^{-5}.

The domain of existence of the axion star solutions for different decay constant f_a in an ADM mass/compactness vs frequency diagram is shown in Fig. 1. Now, and for the remainder of this paper, we focus on axion stars with decay constant $f_a = \{1, 0.035, 0.025, 0.02, 0.017, 0.015\}$. The left panel in Fig. 1 illustrates the distribution of the ADM mass as a function of frequency. The solid lines of various colors represent solutions for different f_a, while the yellow dotted line corresponds to the solution for miniboson stars. The ADM mass M is related to the numerically computed mass $M_{(\mathrm{num})} = \mu M/M_p^2$, where $M_p = \sqrt{\hbar c/G}$ is the Planck mass, and the unit of ADM mass is M_p^2/μ. As f_a increases, the curve of ADM mass variation with frequency becomes closer to that of miniboson stars, suggesting that axion stars decay into miniboson stars when f_a tends to infinity. As mentioned in Eq. (10), when f_a tends to infinity, the self-interaction terms vanish and only the free scalar potential remains; the potential function at this point becomes that of miniboson stars. For larger f_a, the variation of the ADM mass with frequency exhibits a spiral trend. As f_a decreases, this spiral curve transforms into a shape like a duck bill. When f_a is relatively small, the ADM mass has two local maximums, suggesting the potential existence of two stable branches for axion stars. The right panel of Fig. 1 shows the compactness of axion stars varies along the frequency for different f_a. The axion stars become more compact as the frequency decreases for larger f_a. However, when f_a is small, the compactness initially increases with decreasing frequency, then starts decreasing before eventually increasing again.

In order to characterize the region of the stable branch of the axion stars under these six chosen parameters f_a, we show the domain of existence in Fig. 2, displaying both the ADM mass and the Noether charge vs the scalar field frequency. The red solid line represents the Noether charge, while the black solid line represents the ADM mass. We will study the tidal Love numbers under stable configurations. For miniboson stars, the stable branch is determined from the maximum frequency, where the ADM mass M tends to zero, to the maximum ADM mass M [59,60]. However, the domain of stable solutions for axion stars differs from miniboson stars. Considering a self-interaction potential of the scalar field, stability analysis of catastrophe theory has found two stable branches of boson stars [61]. These two branches correspond to compact stars of lower and higher density, respectively. Axion stars with $f_a = 0.02$ were numerically evolved in the study by Herdeiro *et al.* [62], confirming the existence of two stable branches. According to their result, when ADM mass decreases with frequency and $Q\mu^2 > M\mu$, the region is considered stable. For cases with $Q\mu^2 < M\mu$, the solutions with energy excess are unstable. The left panels of Fig. 2 represent cases with one stable branch, highlighted in yellow. The right panels of Fig. 2 represent cases with two stable branches. The stable region at higher frequencies corresponds to the Newtonian stable branch, highlighted in yellow, while the stable region at lower frequencies corresponds to the relativistic stable branch, highlighted in green. Figure 2 reveals that for larger f_a, only one stable branch exists; for smaller f_a values, will exhibit two stable branches. Unlike miniboson stars, axion stars have more compact and stable configurations that depend on different decay constant f_a. Axion stars have two stable branches when $f_a \leq f_a^c$, where $f_a^c = 0.024$ represents the critical parameter for the emergence of the relativistic branch.

The distribution of the scalar field ψ_0 as a function of radial coordinate x is shown in Fig. 3. The left panel illustrates the field function distribution on the Newtonian stable branch at $\omega/\mu = 0.964$, while the right panel displays the field function distribution on the relativistic stable branch at $\omega/\mu = 0.583$. Despite the distribution of the field

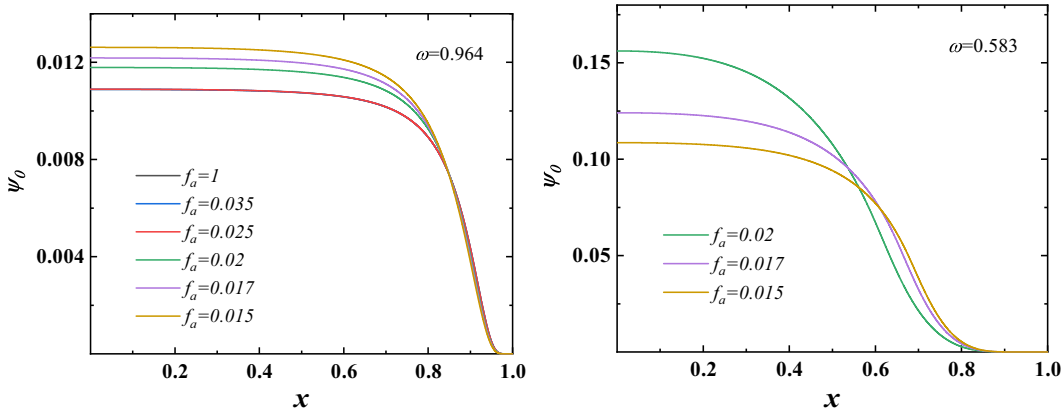

FIG. 3. The distribution of the field function ψ_0 as a function of x at $\omega/\mu = 0.964$ (left panel) and $\omega/\mu = 0.583$ (right panel) for different f_a.

becomes very dilute when close to infinity, it does not completely vanish.

III. TIDAL PERTURBATION

To calculate the tidal Love numbers, we adopt the method in [8,26]. We consider linear perturbations for axion stars immersed in a tidal field, focusing on first-order linear perturbations. In a spherically symmetric background, the perturbed metric can be expressed as

$$g_{\alpha\beta} = g^{(0)}_{\alpha\beta} + h_{\alpha\beta}, \tag{18}$$

where $g^{(0)}_{\alpha\beta}$ is given by Eq. (7). The scalar field under perturbation is

$$\Psi = \Psi^{(0)} + \delta\Psi, \tag{19}$$

with $\Psi^{(0)}$ defined in Eq. (8). The perturbation part of the scalar field is

$$\delta\Psi(t, r, \theta, \varphi) = \sum_{l,m} e^{-i\omega t}\psi_1(r)Y^{\ell m}(\theta, \varphi). \tag{20}$$

The metric perturbations $h_{\alpha\beta}$ can fall into even-parity $h^{(e)}_{\alpha\beta}$ and odd-parity $h^{(o)}_{\alpha\beta}$,

$$h_{\alpha\beta} = h^{(e)}_{\alpha\beta} + h^{(o)}_{\alpha\beta}. \tag{21}$$

In the Regge-Wheeler gauge, $h^{(e)}_{\alpha\beta}$ and $h^{(o)}_{\alpha\beta}$ can be expressed as [63]

$$h^{(e)}_{\alpha\beta} = \begin{pmatrix} e^{\eta(r)}H_0^{\ell m}(r) & 0 & 0 & 0 \\ 0 & e^{\xi(r)}H_2^{\ell m}(r) & 0 & 0 \\ 0 & 0 & r^2K^{\ell m}(r) & 0 \\ 0 & 0 & 0 & r^2\sin^2\theta K^{\ell m}(r) \end{pmatrix} Y^{\ell m}(\theta, \varphi), \tag{22}$$

$$h^{(o)}_{\alpha\beta} = \begin{pmatrix} 0 & 0 & h_0^{\ell m}(r)F_\theta^{\ell m} & h_0^{\ell m}(r)F_\varphi^{\ell m} \\ 0 & 0 & h_1^{\ell m}(r)F_\theta^{\ell m} & h_1^{\ell m}(r)F_\varphi^{\ell m} \\ h_0^{\ell m}(r)F_\theta^{\ell m} & h_1^{\ell m}(r)F_\theta^{\ell m} & 0 & 0 \\ h_0^{\ell m}(r)F_\varphi^{\ell m} & h_1^{\ell m}(r)F_\varphi^{\ell m} & 0 & 0 \end{pmatrix}, \tag{23}$$

where $F_\theta^{\ell m} = -\frac{1}{\sin\theta}\frac{\partial Y^{\ell m}(\theta,\varphi)}{\partial\varphi}$ and $F_\varphi^{\ell m} = \sin\theta\frac{\partial Y^{\ell m}(\theta,\varphi)}{\partial\theta}$. Here, $Y^{\ell m}$ represents spherical harmonics, and for simplicity, we consider $m = 0$ in our subsequent calculations. The Einstein field equations and Klein-Gordon equation under linear perturbations are given by

$$\delta G^\alpha_\beta = 8\pi\delta T^\alpha_\beta, \tag{24}$$

$$\delta\left(\nabla^\alpha\nabla_\alpha\Psi - \frac{\partial V}{\partial|\Psi|^2}\Psi\right) = 0. \tag{25}$$

For nonrotating axion stars, neglecting odd-even perturbation mixing, we can classify tidal deformations into electric and magnetic. Electric tidal deformations have even parity, while magnetic tidal deformations have odd parity. The induced multipole moments are related to the deformation and mass distribution of axion stars, and the tidal Love numbers can be determined through the relationship between multipole moments and induced multipole moments. Considering linear perturbations, the induced multipole moments generated inside axion stars due to tidal deformations are related to the external tidal field's multipole moments. The relationship between ℓ order tidal multipole moments is [64]

$$M_\ell = \lambda_\ell\tilde{E}_\ell,$$
$$S_\ell = \sigma_\ell\tilde{B}_\ell, \tag{26}$$

where λ_ℓ and σ_ℓ are the tidal-polarizability coefficients. M_ℓ and S_ℓ represent the mass and spin multipole moments generated, respectively, and $\tilde{E}_\ell$ and $\tilde{B}_\ell$ represent the electric and magnetic multipole moments of the external tidal field.

To further calculate the tidal Love numbers, we first need to obtain the multipole moments of the tidal field and the induced multipole moments caused by the tidal field. These two types of multipole moments can be extracted through an asymptotic behavior of the metric. We adopt the multipole moment extraction method proposed by Kip S. Thorne [65]. In this method, an asymptotically Cartesian mass-centered coordinate system is chosen, and the (t, t) component and (t, φ) component of the metric can be expressed as

$$g_{tt} = -1 + \frac{2M}{r} + \sum_{\ell\geq 2}\left(\frac{2}{r^{\ell+1}}\left[\sqrt{\frac{4\pi}{2\ell+1}}M_\ell Y^{\ell 0} + (\ell' < \ell \text{pole})\right] - \frac{2}{\ell(\ell-1)} r^l [\tilde{E}_\ell Y^{\ell 0} + (\ell' < \ell \text{pole})]\right),$$
$$g_{t\varphi} = \frac{2J}{r}\sin^2\theta + \sum_{\ell\geq 2}\left(\frac{2}{r^\ell}\left[\sqrt{\frac{4\pi}{2\ell+1}}\frac{S_\ell}{\ell}F_\varphi^{\ell 0} + (\ell' < \ell \text{pole})\right] + \frac{2r^{\ell+1}}{3\ell(\ell-1)}[\tilde{B}_l F_\varphi^{\ell 0} + (\ell' < \ell \text{pole})]\right). \quad (27)$$

Tidal Love numbers are related to the asymptotic behavior of the metric. From the tidal deformability coefficients λ_ℓ and σ_ℓ, we define dimensionless electric tidal Love numbers as k_ℓ^E and magnetic tidal Love numbers as k_ℓ^B [26],

$$k_\ell^E \equiv -\frac{1}{2}\frac{\ell(\ell-1)}{M^{2\ell+1}}\sqrt{\frac{4\pi}{2\ell+1}}\frac{M_\ell}{\tilde{E}_\ell},$$
$$k_\ell^B \equiv -\frac{3}{2}\frac{\ell(\ell-1)}{(\ell+1)M^{2\ell+1}}\sqrt{\frac{4\pi}{2\ell+1}}\frac{S_\ell}{\tilde{B}_\ell}. \quad (28)$$

Here, M represents the mass of the axion stars, and we use $M^{2\ell+1}$ to make the tidal Love numbers dimensionless.

A. Electrical perturbation

We first consider the electric tidal perturbations produced by the external tidal field. By inserting the scalar field perturbation [Eq. (20)] and the even metric perturbation [Eq. (22)] into the linearized Einstein equation from Eq. (24), combining the (θ,θ) and (φ,φ) components of the linearized Einstein equation, we obtain $H_2(r) = H_0(r)$. Using the (r,θ) component, we can express $K'(r)$ as a function of $H_0(r)$ and $\psi_1(r)$:

$$K'(r) = H_0'(r) + H_0(r)\eta'(r) - 32\pi\psi_1(r)\psi_0'(r). \quad (29)$$

Here, $\psi_0(r)$ is obtained from the background solution. By using $K'(r)$ and $H_2(r) = H_0(r)$, we can derive a linear equation for $H_0(r)$ by subtracting the (t,t) component from the (r,r) component of the linearized Einstein equation,

$$a_1 H_0 + a_2 H_0' + H_0'' = a_3\psi_1. \quad (30)$$

Here, a_1, a_2, and a_3 depend on the background solution and are given by

$$a_1 = -32\pi\omega^2\psi_0'^2 - \frac{(\ell^2+\ell)e^\xi}{r^2} + \frac{4\eta'}{r} + \frac{2\xi'}{r} - \frac{\eta'^2}{2} - \frac{\eta'\xi'}{2} + \eta'',$$
$$a_2 = \frac{2}{r} + \frac{\eta'-\xi'}{2},$$
$$a_3 = 32\pi\left[-e^{-\eta+\xi}\omega^2\psi_0 + \psi_0'\left(\frac{2}{r} - \frac{\eta'+\xi'}{2}\right) + \psi_0''\right]. \quad (31)$$

Obtaining the equation for $\psi_1(r)$ from the Klein-Gordon equation under perturbation,

$$b_1\psi_1 + b_2\psi_1' + \psi_1'' = b_3 H_0. \quad (32)$$

Here, b_1, b_2, and b_3 depend on the background solution and are given by

$$b_1 = -\frac{(\ell^2+\ell)e^\xi}{r^2} + e^{-\eta+\xi}\omega^2 - \frac{e^\xi\mu^2\cos\left(\frac{\psi_0}{f_a}\right)}{\sqrt{1-2B+2B\cos\left(\frac{\psi_0}{f_a}\right)}} - \frac{Be^\xi\mu^2\sin^2\left(\frac{\psi_0}{f_a}\right)}{\left[1-2B+2B\cos\left(\frac{\psi_0}{f_a}\right)\right]^{3/2}} - 32\pi\psi_0'^2,$$
$$b_2 = \frac{2}{r} + \frac{\eta'}{2} - \frac{\xi'}{2},$$
$$b_3 = -e^{-\eta+\xi}\omega^2\psi_0 + \frac{2\psi_0'}{r} - \frac{(\eta'+\xi')\psi_0'}{2} + \psi_0''. \quad (33)$$

By imposing appropriate boundary conditions, we can solve the system of equations in Eqs. (30) and (32). To improve the numerical behavior of the perturbation equations near the boundaries and enhance the reliability and accuracy of the calculations, we applied transformations to H_0 and ψ_1:

$$\tilde{H}_0(r) \equiv H_0 r^{-\ell}, \qquad \tilde{\psi}_1(r) \equiv \psi_1 r^{-(\ell+1)}. \quad (34)$$

At the origin $r = 0$, the boundary conditions are given by

$$\tilde{H}_0(0) = \tilde{H}_0^{(\ell)}, \qquad \tilde{H}_0'(0) = 0,$$
$$\tilde{\psi}_1(0) = \tilde{\psi}_1^{(\ell+1)}, \qquad \tilde{\psi}_1'(0) = 0. \quad (35)$$

Since the system is linear, we can choose a specific value for $\tilde{H}_0^{(\ell)}$, such as $\tilde{H}_0^{(\ell)} = 1$. Using the shooting method for

numerical solution [66,67], in order to determine the value of $\tilde{\psi}_1^{(\ell+1)}$, we require $\lim_{r\to\infty}\tilde{\psi}_1(r) \to 0$. Once an reasonable initial value $\tilde{\psi}_1^{(\ell+1)}$ is found, we can use it to obtain nearby solutions. By iterating through this process, one can efficiently get more solutions.

When distances are much larger than the effective radius R, Eq. (30) reduces to

$$H_0'' + \left(\frac{2}{r} + \frac{\eta' - \xi'}{2}\right)H_0' + \left(-\frac{(\ell^2+\ell)e^{\xi}}{r^2} + \frac{4\eta'}{r} + \frac{2\xi'}{r} - \frac{\eta'^2}{2} - \frac{\eta'\xi'}{2} + \eta''\right)H_0 = 0. \tag{36}$$

Using $e^{\eta(r)} = 1\text{–}2M/r = e^{-\xi(r)}$, we obtain

$$H_0'' + \frac{2(r-M)}{r(r-2M)}H_0' + \frac{r(\ell^2+\ell)(2M-r) - 4M^2}{r^2(r-2M)^2}H_0 = 0. \tag{37}$$

We introduce the independent variable $f = r/M - 1$, and Eq. (37) has a general solution,

$$H_0 = E_p P_\ell^2(r/M-1) + E_q Q_\ell^2(r/M-1), \tag{38}$$

where P_ℓ^2 and Q_ℓ^2 represent the associated Legendre function. E_p and E_q are two integration constants, which can be determined by comparing the behavior of H_0 with that of the metric as $r \to \infty$. As $r \to \infty$, the asymptotic forms are

$$\begin{aligned} P_\ell^2 &= a_p(\ell, M)\left(\frac{r}{M}\right)^{\ell} + \mathcal{O}(r^{l-1}), \\ Q_\ell^2 &= a_q(\ell, M)\left(\frac{M}{r}\right)^{\ell+1} + \mathcal{O}(r^{-(l+2)}). \end{aligned} \tag{39}$$

Using Eq. (28), we can express the electrical tidal Love numbers as

$$k_\ell^E = \frac{1}{2}\frac{1}{M^{2\ell+1}}\frac{E_q a_q(\ell, M)}{E_p a_p(\ell, M)}. \tag{40}$$

When calculating the tidal Love numbers at the extraction radius $R_{\rm ext}$ which is far away from the center of axion stars, we define a new function,

$$y = R_{\rm ext}\frac{H_0'(R_{\rm ext})}{H_0(R_{\rm ext})}. \tag{41}$$

For $\ell = 2, 3$, the electric tidal Love numbers are given by

$$\begin{aligned} k_2^E =& \frac{8}{5}(1-2\mathcal{C})^2[2\mathcal{C}(y-1) - y + 2] \\ &\times \left\{2\mathcal{C}(4(y+1)\mathcal{C}^4 + (6y-4)\mathcal{C}^3 + (26-22y)\mathcal{C}^2 + 3(5y-8)\mathcal{C} - 3y + 6)\right. \\ &\left. -3(1-2\mathcal{C})^2(2\mathcal{C}(y-1) - y + 2)\log\left(\frac{1}{1-2\mathcal{C}}\right)\right\}^{-1}, \\ k_3^E =& \frac{8}{7}(1-2\mathcal{C})^2[2(y-1)\mathcal{C}^2 - 3(y-2)\mathcal{C} + y - 3] \\ &\times \left\{2\mathcal{C}[4(y+1)\mathcal{C}^5 + 2(9y-2)\mathcal{C}^4 - 20(7y-9)\mathcal{C}^3 + 5(37y-72)\mathcal{C}^2 - 45(2y-5)\mathcal{C} + 15(y-3)\right. \quad] \\ &\left. -15(1-2\mathcal{C})^2(2(y-1)\mathcal{C}^2 - 3(y-2)\mathcal{C} + y - 3)\log\left(\frac{1}{1-2\mathcal{C}}\right)\right\}^{-1}, \end{aligned} \tag{42}$$

where $\mathcal{C} = M/R_{\rm ext}$. k_2 and k_3 are quadrupolar and octupolar electric tidal Love numbers, respectively.

B. Magnetic perturbation

Next, we consider the magnetic tidal perturbations in the tidal environment. The earliest magnetic Love numbers for neutron stars were computed by Binnington and Poisson (BP) and Damour and Nagar (DN) using different methods, resulting in sign differences in the obtained results [8,9]. BP's method [9] assumed the fluid is strictly static, requiring complete absence of internal motion, and derived all perturbation equations using static fluid analysis, yielding positive magnetic Love numbers. DN [8] did not rederive the perturbation equations but instead computed the Regge-Wheeler equation and then took the static limit $\omega \to 0$, under which the fluid is irrotational [68,69], allowing for internal motion driven by gravitomagnetic interaction with the tidal environment, resulting in negative magnetic Love numbers. We adopt the method used by DN [8] to compute the magnetic Love

numbers, utilizing Schwarzschild coordinates and the Regge-Wheeler gauge.

Applying the same steps as used for computing the electric tidal Love numbers, we first utilize Eqs. (20) and (23) within Eq. (24). This yields $\psi_0 = 0$ from the (r,θ) component and provides the equation for h_0 from the (t,φ) component,

$$c_1 h_0(r) + c_2 h_0'(r) + h_0''(r) = 0, \tag{43}$$

where c_1 and c_2 are defined as

$$c_1 = \frac{-e^{\xi}(\ell^2+\ell-2) + r(\eta'+\xi') - 2}{r^2},$$
$$c_2 = -\frac{\xi'+\eta'}{2}. \tag{44}$$

We perform a transformation on h_0 to remove its explicit dependence on r,

$$\tilde{h}_0(r) \equiv h_0 r^{\ell+1}. \tag{45}$$

Under this transformation, the boundary conditions at the origin $r = 0$ become

$$\tilde{h}_0(0) = \tilde{h}_0^{(\ell+1)}, \qquad \tilde{h}_0'(0) = 0. \tag{46}$$

When distances are much larger than the effective radius R, and using $e^{\eta(r)} = 1\text{–}2M/r = e^{-\xi(r)}$, Eq. (43) simplifies to

$$\frac{4M - \ell(\ell+1)}{r^2(r-2M)} h_0'(r) + h_0''(r) = 0. \tag{47}$$

The solution to this differential equation is

$$h_0 = B_f \frac{r^2}{4M^2}\,{}_2F_1\left(1-\ell, 2+\ell; 4; \frac{r}{2M}\right) + B_g G^{20}_{22}\left(\frac{r}{2M}\middle| \begin{matrix} 1-\ell, & 2+\ell \\ -1, & 2 \end{matrix}\right). \tag{48}$$

Here, B_f and B_g are integration constants, ${}_2F_1$ represents the hypergeometric function, and G^{20}_{22} represents the Meijer function. As $r \to \infty$, the asymptotic behavior is

$$h_0 = B_f b_f(\ell, M)\left(\frac{r}{M}\right)^{\ell+1} + \mathcal{O}(r^{-l-1}) + B_g b_g(\ell, M)\left(\frac{M}{r}\right)^{\ell} + \mathcal{O}(r^l). \tag{49}$$

Using Eq. (28), we can express the magnetic tidal Love numbers as

$$k_\ell^B = -\frac{1}{2}\frac{\ell}{\ell+1}\frac{1}{M^{2\ell+1}}\frac{B_g b_g(\ell, M)}{B_f b_f(\ell, M)}. \tag{50}$$

By combining this with the asymptotic behavior of the metric's (t,φ) component, we can derive the expressions for k_2^B (quadrupolar) and k_3^B (octupolar) magnetic tidal Love numbers when $\ell = 2, 3$ as follows:

$$k_2^B = \frac{8}{5}\frac{2\mathcal{C}(y-2) - y + 3}{2\mathcal{C}[2\mathcal{C}^3(y+1) + 2\mathcal{C}^2 y + 3\mathcal{C}(y-1) - 3y + 9] + 3[2\mathcal{C}(y-2) - y + 3]\log(1-2\mathcal{C})},$$
$$k_3^B = \frac{8}{7}(8\mathcal{C}^2(y-2) - 10\mathcal{C}(y-3) + 3(y-4))(15[8\mathcal{C}^2(y-2) - 10\mathcal{C}(y-3) + 3(y-4)]\log(1-2\mathcal{C}) + 2\mathcal{C}[4\mathcal{C}^4(y+1) + 10\mathcal{C}^3 y + 30\mathcal{C}^2(y-1) - 15\mathcal{C}(7y-18) + 45(y-4)])^{-1}, \tag{51}$$

where $y = R_{\rm ext} h_0'(R_{\rm ext})/h_0(R_{\rm ext})$ and $\mathcal{C} = M/R_{\rm ext}$.

IV. TIDAL LOVE NUMBERS OF AXION STARS

In this section, we will study the tidal Love numbers of spherically symmetric axion stars by computing y and $\mathcal{C}$ at extraction radius $R_{\rm ext}$. It is noted that in Sec. II the first three parameters, characterized by larger values of f_a, exhibit only one stable branch known as the Newtonian stable branch. Conversely, for the latter three cases with smaller f_a, the system displays the presence of two stable branches. The branch from the maximum frequency to the first local maximum mass corresponds to the Newtonian stable branch, while the relativistic stable branch corresponds to the other stable branch.

First, we analyze tidal Love numbers on the Newtonian stable branch. We calculate both the quadrupolar Love numbers ($\ell = 2$) and the octupolar Love numbers ($\ell = 3$). In Fig. 4, the left panels show the electric tidal Love numbers k_ℓ^E, while the right panels exhibit the magnetic tidal Love numbers k_ℓ^B as functions of the axion stars mass M for different parameter f_a. The top panels correspond to the quadrupole case ($\ell = 2$), whereas the bottom panels represent the octupole case ($\ell = 3$).

On the Newtonian stable branch for $\ell = 2$, we observe that the electric tidal Love numbers k_2^{E-N} decrease with

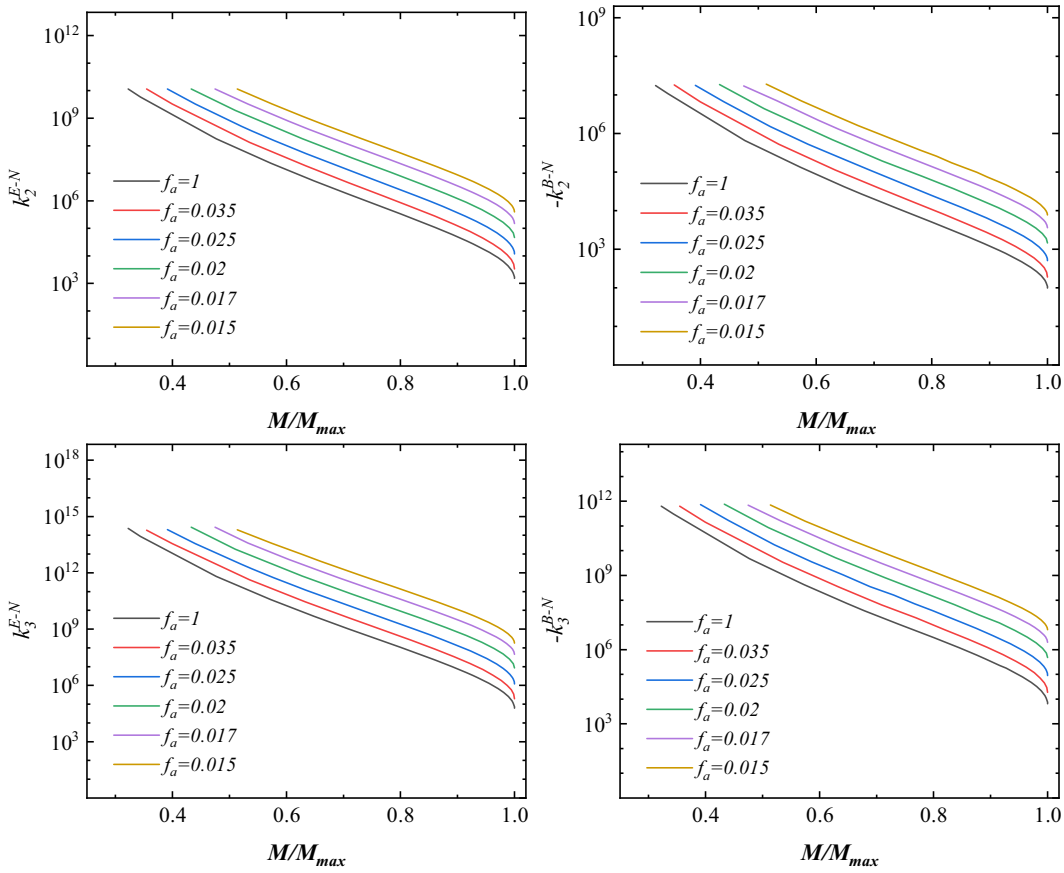

FIG. 4. Tidal Love numbers for axion stars on the Newtonian stable branch, including the electric type (left) and magnetic type (right). The top panels represent the quadrupolar tidal Love numbers ($\ell = 2$), while the bottom panels depict the octupolar tidal Love numbers ($\ell = 3$).

increasing mass under the same parameter f_a. As the mass increases, the axion stars become very compact, and compactness reaches maximum at $M/M_{\max} = 1$, where k_2^{E-N} reaches its minimum. On the other hand, the absolute value of the magnetic tidal Love numbers k_2^{B-N} decreases with increasing mass. The variation in the parameter f_a does not alter the general trend of the tidal Love numbers with mass.

For a constant mass ratio $M/M_{\max}$, the self-interaction of the axion potential becomes stronger and quadrupole tidal Love numbers become larger as the parameter f_a decreases, suggesting increased tidal deformability as f_a decreases. The electric tidal Love numbers are positive on this branch suggesting a positive feedback from the additional potential induced by the external gravitational field, promoting deformation. The negative magnetic tidal Love numbers show that the external tidal field produces a deformation in the gravitational potential that works against these deformations. At a consistent mass ratio, the magnitude of the magnetic tidal Love numbers is observed to be smaller than that of the electric tidal Love numbers. We also perform calculations for the case of $\ell = 3$ and obtain results similar to those for $\ell = 2$.

Next, we investigate the situation on the relativistic stable branch of axion stars. Tidal Love numbers for axion stars on the relativistic stable branch are presented in Fig. 5. The trends of tidal Love numbers with respect to mass on the relativistic stable branch are similar to those observed on the Newtonian stable branch. The electric tidal Love numbers k_2^{E-R} and the absolute value of the magnetic tidal Love numbers k_2^{B-R} decrease as the mass increases. On this branch, the electric tidal Love numbers are positive, and the magnetic tidal Love numbers are negative. However, unlike the Newtonian stable branch, on the relativistic stable branch, for the same mass ratio, electric k_2^{E-R} and magnetic k_2^{B-R} Love numbers have nearly equal magnitudes, especially as $M/M_{\max} \to 1$, where they are almost identical. For a given parameter f_a and the same mass ratio, the electric tidal Love numbers are always greater than magnetic tidal Love numbers. Furthermore, the Love numbers on the relativistic stable branch are markedly smaller than those on the Newtonian stable branch, indicating significantly weaker tidal deformability of axion stars on the relativistic stable branch compared to the Newtonian stable branch. At $M/M_{\max} = 1$, k_2^{E-R} and k_2^{B-R} tend to approach zero. This may be attributed to the more compact configurations of

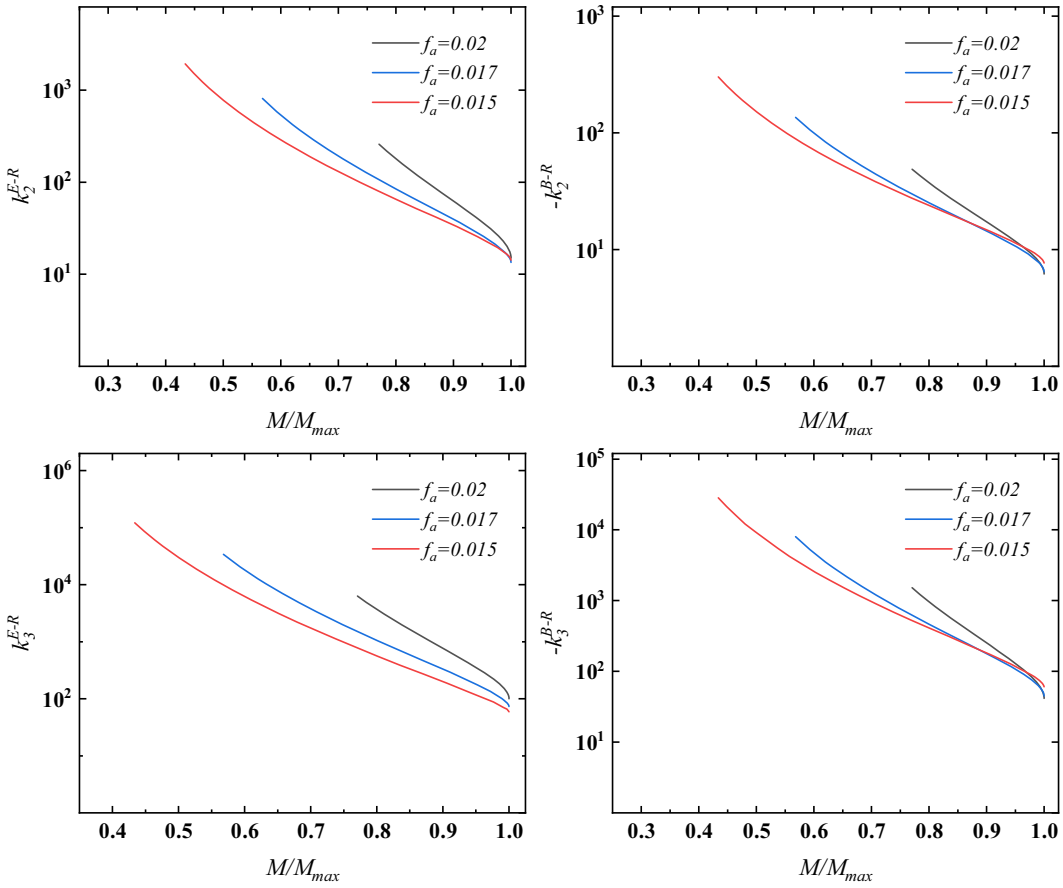

FIG. 5. Tidal Love numbers for axion stars on the relativistic stable branch, including the electric type (left) and magnetic type (right). The top panels represent the quadrupolar tidal Love numbers ($\ell = 2$), while the bottom panels depict the octupolar tidal Love numbers ($\ell = 3$).

axion stars on the relativistic stable branch, resulting hardly distorted compared to those on the Newtonian stable branch.

V. CONCLUSIONS

In this paper, we briefly reviewed the domain of existence of the spherically symmetric axion stars solutions, considering the self-interaction complex scalar field minimally coupled to Einstein's gravity. As the value of f_a increases, the self-interaction become weaker and the mass-frequency curve of axion stars approaches more closely to that of miniboson stars, implying that axion stars decay into miniboson stars as f_a approaches infinity. As f_a decreases the self-interaction strengthens and the mass-frequency relation changes from a spiral shape to a "duck-bill" curve. For miniboson stars, there is only one stable branch, while axion stars at $f_a \leq 0.024$ exhibit a new stable branch that becomes more compact. The Newtonian stable branch extends from the maximum frequency to the first local maximum mass, while the relativistic stable branch extends from the second $Q\mu^2 = M\mu$ to the second mass local maximum. An unstable branch connects the Newtonian and relativistic stable branches, with axion stars having greater compactness under the relativistic stable branch.

Subsequently, we investigated deformability and the corresponding tidal Love numbers which fall into electric type (even parity) and magnetic type (odd parity). We have numerically solved the ordinary differential equations using the finite element method. Expressions for the Love numbers of axion stars were derived through perturbations to the Einstein equations when considering the radius far away from the center of axion stars. Following this, six distinct decay constants f_a were chosen, and computations were conducted for the quadrupole tidal Love numbers ($\ell = 2$) as well as the octupole tidal Love numbers ($\ell = 3$). The results reveal that on the stable branch, whether Newtonian or relativistic, the electric tidal Love numbers are positive while the magnetic tidal Love numbers are negative. These indicate that even parity perturbations lead to the deformation of gravitational potential that enhances the deformation. However, the gravitational potential deformations were caused by odd parity perturbations against these deformations. The electric tidal Love numbers are larger than the magnetic tidal Love numbers. With an increase in mass, there is a corresponding decrease in the

tidal Love numbers. Those results are similar with boson stars and Proca stars [26,37]. However, on the Newtonian stable branch, the electric tidal Love numbers are significantly larger than the magnetic ones, whereas on the relativistic branch, the electric tidal Love numbers only slightly exceed the magnetic ones. Furthermore, the tidal Love numbers on the relativistic stable branch are much smaller than those on the Newtonian stable branch, and as $M/M_{\max} \to 1$ on the relativistic branch, the tidal Love numbers tend to approach zero. This intriguing result suggests that at the maximum mass on the relativistic branch, the tidal Love numbers reach their minimum values. Because of the more compact configurations of axion stars immersed in external tidal fields, smaller mass and spin multipole moments are produced, thereby resulting in weakened tidal deformability.

Rotating axion boson stars as the spinning generalizations of static axion boson stars have been constructed in [54]. Extending our study to investigate the tidal Love numbers of rotating axion boson stars and multifield axion boson stars would be interesting. Additionally, recent studies indicate that the excited boson stars can stabilize when considering self-interactions [70,71]. Therefore, investigating the tidal deformability of ground states and excited states in such self-interacting spherically symmetric configurations is highly meaningful.

ACKNOWLEDGMENTS

This work is supported by National Key Research and Development Program of China (Grant No. 2020YFC2201503) and the National Natural Science Foundation of China (Grants No. 12275110 and No. 12247101). Parts of computations were performed on the Shared Memory system at Institute of Computational Physics and Complex Systems in Lanzhou University.

[1] P. Goldreich and S. Peale, Astrophys. J. **71**, 425 (1966).
[2] A. Toomre and J. Toomre, Astrophys. J. **178**, 623 (1972).
[3] A. E. H. Love, Proc. R. Soc. A **82**, 73 (1909).
[4] A. E. H. Love, *Some Problems of Geodynamics* (Cambridge University Press, Cambridge, England, 1911).
[5] T. Shida, Proc. Tokyo Math.-Phys. Soc. **6**, 242 (1912).
[6] T. Hinderer, Astrophys. J. **677**, 1216 (2008).
[7] E. E. Flanagan and T. Hinderer, Phys. Rev. D **77**, 021502 (2008).
[8] T. Damour and A. Nagar, Phys. Rev. D **80**, 084035 (2009).
[9] T. Binnington and E. Poisson, Phys. Rev. D **80**, 084018 (2009).
[10] T. Hinderer, A. Taracchini, F. Foucart, A. Buonanno, J. Steinhoff, M. Duez, L. E. Kidder, H. P. Pfeiffer, M. A. Scheel, B. Szilagyi *et al.*, Phys. Rev. Lett. **116**, 181101 (2016).
[11] T. Dietrich, T. Hinderer, and A. Samajdar, Gen. Relativ. Gravit. **53**, 27 (2021).
[12] K. Yagi and N. Yunes, Science **341**, 365 (2013).
[13] K. Yagi and N. Yunes, Phys. Rev. D **88**, 023009 (2013).
[14] P. Pani, L. Gualtieri, A. Maselli, and V. Ferrari, Phys. Rev. D **92**, 024010 (2015).
[15] P. Pani, L. Gualtieri, and V. Ferrari, Phys. Rev. D **92**, 124003 (2015).
[16] P. Landry and E. Poisson, Phys. Rev. D **92**, 124041 (2015).
[17] P. Landry and E. Poisson, Phys. Rev. D **91**, 104018 (2015).
[18] P. Landry, Phys. Rev. D **95**, 124058 (2017).
[19] P. Landry, arXiv:1805.01882.
[20] P. K. Gupta, J. Steinhoff, and T. Hinderer, Phys. Rev. Res. **3**, 013147 (2021).
[21] R. X. Yang, F. Xie, and D. J. Liu, Universe **8**, 576 (2022).
[22] L. Meng and D. J. Liu, Astrophys. Space Sci. **366**, 105 (2021).
[23] H. Fang and G. Lovelace, Phys. Rev. D **72**, 124016 (2005).
[24] N. Gürlebeck, Phys. Rev. Lett. **114**, 151102 (2015).
[25] E. Poisson, Phys. Rev. D **91**, 044004 (2015).
[26] V. Cardoso, E. Franzin, A. Maselli, P. Pani, and G. Raposo, Phys. Rev. D **95**, 084014 (2017).
[27] N. Sennett, T. Hinderer, J. Steinhoff, A. Buonanno, and S. Ossokine, Phys. Rev. D **96**, 024002 (2017).
[28] V. Cardoso and P. Pani, Living Rev. Relativity **22**, 4 (2019).
[29] J. A. Wheeler, Phys. Rev. **97**, 511 (1955).
[30] D. J. Kaup, Phys. Rev. **172**, 1331 (1968).
[31] R. Ruffini and S. Bonazzola, Phys. Rev. **187**, 1767 (1969).
[32] W. Hu, R. Barkana, and A. Gruzinov, Phys. Rev. Lett. **85**, 1158 (2000).
[33] V. Sahni and L. M. Wang, Phys. Rev. D **62**, 103517 (2000).
[34] T. Matos and L. A. Urena-Lopez, Classical Quantum Gravity **17**, L75 (2000).
[35] L. Hui, J. P. Ostriker, S. Tremaine, and E. Witten, Phys. Rev. D **95**, 043541 (2017).
[36] R. F. P. Mendes and H. Yang, Classical Quantum Gravity **34**, 185001 (2017).
[37] C. A. R. Herdeiro, G. Panotopoulos, and E. Radu, J. Cosmol. Astropart. Phys. 08 (2020) 029.
[38] N. Uchikata, S. Yoshida, and P. Pani, Phys. Rev. D **94**, 064015 (2016).
[39] P. Pani, Phys. Rev. D **92**, 124030 (2015); **95**, 049902(E) (2017).
[40] S. Postnikov, M. Prakash, and J. M. Lattimer, Phys. Rev. D **82**, 024016 (2010).
[41] M. B. Albino, R. Fariello, and F. S. Navarra, Phys. Rev. D **104**, 083011 (2021).
[42] S. Davidson and T. Schwetz, Phys. Rev. D **93**, 123509 (2016).
[43] H. Baer, K. Y. Choi, J. E. Kim, and L. Roszkowski, Phys. Rep. **555**, 1 (2015).
[44] V. B. Klaer and G. D. Moore, J. Cosmol. Astropart. Phys. 11 (2017) 049.

[45] J. Eby, M. Leembruggen, J. Leeney, P. Suranyi, and L. C. R. Wijewardhana, J. High Energy Phys. 04 (2017) 099.
[46] F. Wilczek, Phys. Rev. Lett. **40**, 279 (1978).
[47] R. D. Peccei and H. R. Quinn, Phys. Rev. Lett. **38**, 1440 (1977).
[48] S. Weinberg, Phys. Rev. Lett. **40**, 223 (1978).
[49] C. G. Callan, Jr., R. F. Dashen, and D. J. Gross, Phys. Rev. D **20**, 3279 (1979).
[50] R. Essig, J. A. Jaros, W. Wester, P. Hansson Adrian, S. Andreas, T. Averett, O. Baker, B. Batell, M. Battaglieri, J. Beacham *et al.*, arXiv:1311.0029.
[51] A. Arvanitaki, S. Dimopoulos, S. Dubovsky, N. Kaloper, and J. March-Russell, Phys. Rev. D **81**, 123530 (2010).
[52] P. Svrcek and E. Witten, J. High Energy Phys. 06 (2006) 051.
[53] D. Guerra, C. F. B. Macedo, and P. Pani, J. Cosmol. Astropart. Phys. 09 (2019) 061; 06 (2020) E01.
[54] J. F. M. Delgado, C. A. R. Herdeiro, and E. Radu, J. Cosmol. Astropart. Phys. 06 (2020) 037.
[55] Y. B. Zeng, H. B. Li, S. X. Sun, S. Y. Cui, and Y. Q. Wang, Eur. Phys. J. C **84**, 187 (2024).
[56] S. L. Liebling and C. Palenzuela, Living Rev. Relativity **26**, 1 (2023).
[57] G. Grilli di Cortona, E. Hardy, J. Pardo Vega, and G. Villadoro, J. High Energy Phys. 01 (2016) 034.
[58] F. E. Schunck and E. W. Mielke, Classical Quantum Gravity **20**, R301 (2003).
[59] T. D. Lee and Y. Pang, Nucl. Phys. **B315**, 477 (1989).
[60] M. Gleiser, Phys. Rev. D **38**, 2376 (1988); **39**, 1257 (1989).
[61] B. Kleihaus, J. Kunz, and S. Schneider, Phys. Rev. D **85**, 024045 (2012).
[62] C. A. R. Herdeiro, A. M. Pombo, E. Radu, P. V. P. Cunha, and N. Sanchis-Gual, J. Cosmol. Astropart. Phys. 04 (2021) 051.
[63] T. Regge and J. A. Wheeler, Phys. Rev. **108**, 1063 (1957).
[64] T. Damour, M. Soffel, and C. m. Xu, Phys. Rev. D **45**, 1017 (1992).
[65] K. S. Thorne, Rev. Mod. Phys. **52**, 299 (1980).
[66] W. H. Press, S. A. Teukolsky, W. T. Vetterling, and B. P. Flannery, *Numerical Recipes in C: The Art of Scientific Computing* (Cambridge University Press, Cambridge, England, 1992).
[67] C. F. B. Macedo, P. Pani, V. Cardoso, and L. C. B. Crispino, Phys. Rev. D **88**, 064046 (2013).
[68] P. Landry and E. Poisson, Phys. Rev. D **91**, 104026 (2015).
[69] P. Pani, L. Gualtieri, T. Abdelsalhin, and X. Jiménez-Forteza, Phys. Rev. D **98**, 124023 (2018).
[70] M. Brito, C. Herdeiro, E. Radu, N. Sanchis-Gual, and M. Zilhão, Phys. Rev. D **107**, 084022 (2023).
[71] N. Sanchis-Gual, C. Herdeiro, and E. Radu, Classical Quantum Gravity **39**, 064001 (2022).